

SPS ELECTRON CLOUD HEAT LOAD MEASUREMENTS WITH WAMPAC AND SIMULATIONS

V. Baglin and B. Jenninger, CERN, 1211 Geneva 23, Switzerland.

Abstract

A calorimeter, WAMPAC, operating at room temperature has been designed and installed into the SPS to measure directly the electron cloud induced heat load due to the LHC type proton beam. Theoretical behaviour, calibrations, measurement protocols, preliminary results and simulation benchmarking are presented. Scaling of the results to the LHC indicated a linear heating power in a LHC dipole of about $500 \text{ mW}\cdot\text{m}^{-1}$ for $5 \cdot 10^{10}$ protons.bunch⁻¹ for a copper surface which is not fully conditioned (maximum of secondary electron yield ~ 1.9).

1 INTRODUCTION

In the cryogenic elements of the Large Hadron Collider (LHC), the proton beams will be contained inside a perforated 'beam screen' (BS), cooled at a temperature between $\sim 5 \text{ K}$ and 20 K . Apart to provide pumping, the BS is necessary to intercept the beam induced heat loads such as synchrotron radiation (SR), photoelectrons and resistive wall losses, in order to avoid their dissipation in the 1.9 K cold bore (CB) of the superconducting magnets. Electrons liberated into the beam vacuum chamber are accelerated towards the beam screen due to the electric field of a passing proton bunch. The impact energy of the electrons on the wall produces secondary electrons that may lead to a build up of an electron cloud due to the successive bunches [1]. Preliminary estimations of the heat load deposited by the electron cloud onto the beam screen indicated a non negligible contribution to the total heat load budget [1, 2, 3]. Last estimations, including elastic reflection of electrons, give linear heat input in the LHC arc dipole of $3.5 \text{ W}\cdot\text{m}^{-1}$ for an unscrubbed copper surface and $0.22 \text{ W}\cdot\text{m}^{-1}$ for a fully scrubbed surface [4]. In the dipole assembly at ~ 5 to 20 K temperature level, the installed cooling power is $1.13 \text{ W}\cdot\text{m}^{-1}$ per aperture [5]. At nominal beam current, the total heat load budget is $0.72 \text{ W}\cdot\text{m}^{-1}$ per aperture. The allocation to electron cloud is 28 % *i.e.* $\sim 0.22 \text{ W}\cdot\text{m}^{-1}$ for the dipole field region and 22 % *i.e.* $\sim 1.9 \text{ W}\cdot\text{m}^{-1}$ for the field free region [6]. An electron cloud activity has been observed in the SPS with LHC type beams [7]. It is therefore of great importance to measure the heat load deposited by this multipacting effect, in order to benchmark the simulations. For this purpose the WArm MultiPActing Calorimeter (WAMPAC), which

measures directly the beam induced heat, was installed at the beginning of 2001 in section 417, long straight section 4, of the SPS.

2 PRINCIPLES

The calorimeter consists of a thermally floating copper screen, which is installed inside the SPS LSS type vacuum chamber. This screen is equipped with temperature sensors (thermocouple type E) and a heater for calibration of the calorimeter. The heat load into the calorimeter is measured as a function of the temperature evolution of the screen.

2.1 Heat equations

Physically, the heat input to the screen is balanced by the thermal resistance through radiative and contact heat losses and by the warming up of the screen. The dynamic behaviour is described with the differential equation below :

$$\dot{Q} - R \cdot \Delta T - C \dot{\Delta T} = 0 \quad (1)$$

\dot{Q} is the heat load on the screen, ΔT is the temperature difference between copper screen T and vacuum chamber T_v , R is the thermal resistance between screen and vacuum chamber and C is the thermal capacitance of the screen

Since initially there is no temperature difference between the copper screen and the vacuum chamber *i.e.* $\Delta T(t=0) = 0$ and since at equilibrium $\dot{\Delta T} = 0$, the solution of the differential equation is:

$$\Delta T(t) = \dot{Q} \cdot R \cdot \left(1 - e^{-\frac{t}{RC}} \right) \quad (2)$$

With the time constant:

$$\tau = RC \quad (3)$$

The slope is :

$$\frac{d\Delta T(t)}{dt} = \frac{\dot{Q}}{C} \cdot e^{-\frac{t}{RC}} \quad (4)$$

The thermal resistance R is defined by the two resistances in parallel of the thermal radiation, R_{Rad} and the thermal contact, R_{cond} :

$$R = \frac{R_{\text{Rad}} R_{\text{cond}}}{R_{\text{Rad}} + R_{\text{cond}}} \quad (5)$$

For small temperature differences ΔT between the copper screen and the vacuum chamber, the radiative heat flow \dot{Q}_R versus the vacuum envelope is :

$$\dot{Q}_R = \sigma \varepsilon S F (T^4 - T_v^4) \approx \sigma \varepsilon S F 4T^3 \Delta T \quad (6)$$

where $\sigma = 5.67 \cdot 10^{-8} \text{ W.m}^{-2}.\text{K}^{-4}$ is the Stefan-Boltzmann-Constant, ε is the effective emissivity, F is the view factor between screen and vacuum chamber, S is the surface area of the copper screen 'seen' by the vacuum chamber.

Thus, by definition, the radiative thermal resistance is:

$$R_{Rad} = \frac{\Delta T}{\dot{Q}_R} \approx \frac{1}{\sigma \varepsilon S F 4T^3} \quad (7)$$

The copper screen is centred inside the vacuum chamber with small stainless steel screws at each end. The conductive resistance between screen and vacuum chamber is dominated by the contacts, which makes it difficult to estimate beforehand the conductive thermal resistance by a purely analytical approach. The approach taken was to measure the electrical resistance. The similarity of the mechanisms of thermal and electrical conduction in metals therefore relates the conductive thermal resistance R_{cond} and electrical resistance R_{el} [8]. For stainless steel and at room temperature: $\lambda \sim 15 \text{ W.m}^{-1}.\text{K}^{-1}$ (thermal conductivity) and $\rho \sim 7 \cdot 10^{-7} \Omega.\text{m}$ (electrical resistivity).

$$R_{cond} \approx \frac{R_{el}}{\lambda \rho} \quad (8)$$

The thermal capacitance, C , is defined by specific heat of copper c times the mass of the copper screen M :

$$C = c M \quad (9)$$

2.2 Measurements

The only expected measurable beam induced heat load is due to the electron cloud activity because heat input from image currents are negligible and estimated to be about 5 mW.m^{-1} for the nominal LHC beam in SPS (4 batches of 72 bunches at 10^{11} protons.bunch $^{-1}$). Figure 1 shows an ideal measurement cycle for this set-up where the relative temperature is plotted versus time. For the analysis of the measurements only temperature changes are taken into account, and not the absolute values. When heat is deposited onto the copper screen, the relative temperature increases, following the thermal capacity, up to an equilibrium defined by the thermal resistance. When the heat load is suppressed, the system cools down back to the initial value.

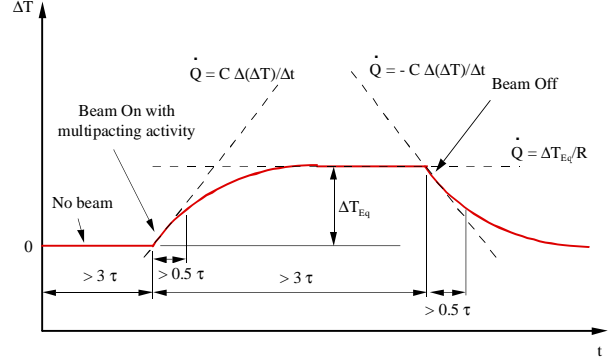


Figure 1 : Ideal measurement cycle.

Two independent methods are used to determine the heat load from an ideal measurement cycle:

1. Using (4) at $t = 0$, the measure of the initial warm-up slope, which is determined by the thermal capacitance of the copper screen, allows to compute the heat load. To avoid uncertainty in the measurement due to temperature instability, the slope is measured during the first hour of warming up which gives an accuracy of 30 % (if the temperature were stable, a slope measured during 5 minutes will give an accuracy better than 5 %). The start of the cool-down slope from equilibrium is identical to the warm-up slope, but with negative sign (equation (1) with the following boundary conditions : $\Delta T(t = 0) = \dot{Q} \cdot R$ and $\Delta T(t = \infty) = 0$).

$$\dot{Q} = C \frac{\Delta(\Delta T)}{\Delta t} \quad (10)$$

2. Using (2) at $t = \infty$, the measure of the equilibrium temperature ΔT_{Eq} , which is determined by the thermal conductance to the vacuum envelope, allows to compute the heat load. In this case, the equilibrium temperature is measured after 3 hours of constant beam condition which gives about 70 % of the correct value.

$$\dot{Q} = \frac{\Delta T_{Eq}}{R} \quad (11)$$

3 EXPERIMENTAL SETUP

3.1 Description

Figure 2 shows a schematic of the experimental set-up. A circular OFHC copper screen is installed inside an SPS vacuum chamber. This screen is 1.3 m long, 0.14 m diameter and 0.5 mm thick. The screen has been cleaned according to CERN standard procedure. It is equipped with 5, type E, thermocouples (TC1, TC2, TC3, TC4 and TC5), which are equally distributed over the length. A calibration heater was brazed over the full length of the screen. Additional thermocouples are installed on the vacuum chamber (TC6) and suspended in the air (TC7) around the experiment. A calibrated Bayard-

Alpert vacuum gauge, type 305, and a pick-up electrode are installed close to the copper screen to detect the electron cloud activity identified by the pressure rise of the system due to electron stimulated desorption. A solenoid coil, wrapped around the vacuum chamber can be powered to attenuate the multipacting activity. Since the multipacting threshold is lower in a dipole field [9], permanent dipole magnets (~ 0.05 T) have been installed over a length of 0.7 m to trigger multipacting at a lower beam current than in field free region. Indeed, part of the current limitation in the SPS is due to strong ESD observed in the dipole regions. The data acquisition was performed with a dedicated LabVIEW software. About 100 measurements are averaged and logged every 5 minutes.

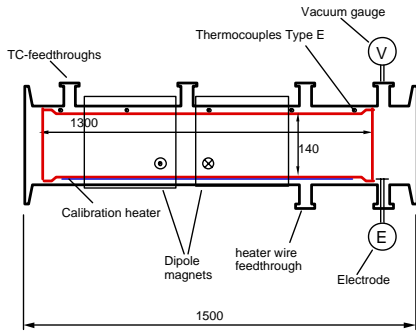


Figure 2: Schematic of the WAMPAC calorimeter

Figure 3 shows photographs of the WAMPAC copper screen and the WAMPAC experiment installed into the SPS.



Figure 3: Photographs of the WAMPAC copper screen and of WAMPAC installed in the SPS section 417 with and without dipole magnets.

3.2 Theoretical thermal properties

The time constant, thermal resistance and thermal capacitance could be computed and compared with calibration data using (3), (5), (9) and standard data from copper (emissivity, $\varepsilon = 0.05$, specific heat of copper, $c = 400 \text{ J.kg}^{-1}.\text{K}^{-1}$). The view factor, F , of the copper screen inserted into the SPS chamber is

assumed to be unity. The copper screen mass, M , is 3 kg, has a surface area, S , of 0.6 m^2 and operates at $T = 293 \text{ K}$ (Stefan-Boltzmann constant $\sigma = 5.67 \cdot 10^{-8} \text{ W.m}^{-2}.\text{K}^{-4}$). The measured electrical resistance between screen and vacuum chamber was $0.5 \text{ m}\Omega$, corresponding to conductive thermal resistance of $R_{cond} \sim 48 \text{ K.W}^{-1}$. The radiative thermal resistance is $R_{rad} \sim 6 \text{ K.W}^{-1}$. The total thermal resistance R is therefore dominated by radiation. The corresponding theoretical thermal capacitance, C , resistance, R and time constant, τ are shown in Table 1.

Table 1 : Theoretical thermal capacitance, C , thermal resistance, R and time constant τ .

C (J.K^{-1})	R (K.W^{-1})	τ (hours)
1200	6	2

3.3 Effect of dipole field on temperature homogeneity

With the additional dipole field, the heat deposition into the copper screen is not homogeneous. The heat is only deposited along the magnetic fields *i.e.* maximum heat deposition at the poles. Longitudinally the heat is mainly deposited in the region with magnetic field, because of the lower multipacting threshold in the magnetic field region. Therefore, both the thermal diffusion time constants (azimuthal and longitudinal) have to be considered, and have to be smaller than the warmup time constant of the system.

The one dimensional diffusion time constant is related to the thermal diffusivity by (12). The thermal diffusivity being the ratio of the thermal conductivity, λ , to the product of the material density, ρ by the specific heat, c . For copper ($\lambda = 400 \text{ W.m}^{-1}.\text{K}^{-1}$ and $\rho = 8900 \text{ kg.m}^{-3}$), the thermal diffusivity equals $1.1 \cdot 10^{-4} \text{ m}^2.\text{s}^{-1}$.

$$\tau_D = \frac{L^2}{D} = \frac{L^2}{\lambda / \rho c} \quad (12)$$

This diffusion time constant is a measure of the time delay to a change in temperature of a point at the distance L from the heat source. Azimuthally, the distance L is about the quarter of the tube circumference (*i.e.* $L_A \sim 0.11 \text{ m}$) and longitudinally it is the length between the end of the magnetic field region and the end of the tube (*i.e.* $L_L \sim 0.3 \text{ m}$), therefore :

- the azimuthal diffusion time constant is: $\tau_{DA} = 110 \text{ s}$
- the longitudinal time constant is: $\tau_{DL} = 820 \text{ s}$

Thus, both diffusion time constants are small compared to the system time constant, τ , of 2 hours.

Similarly, to get a homogenous temperature on the copper screen under steady state conditions, the longitudinal and azimuthal thermal resistance of the screen has to be small compared with the the local thermal resistance versus the vacuum envelope.

For a copper screen diameter of 0.14 m and a thickness of 0.5 mm and using for the azimuthal and longitudinal resistance the same lengths as for the diffusion time constants, we get the following thermal resistances:

- azimuthal thermal resistance: $R_A = 0.9 \text{ K.W}^{-1}$
- longitudinal thermal resistance : $R_L = 3.4 \text{ K.W}^{-1}$

The thermal resistances are still small compared with the resistance versus the vacuum envelope for the same area and does therefore not yet significantly modify the temperature homogeneity. A further reduction of the wall thickness, however, might have a non-negligible influence on the steady state temperature distribution.

3.4 Calibration and sensitivity

The precise values of the thermal capacitance and resistance can be determined during an *in-situ* calibration using the linear heater by applying a known heat load. From equation (10), the thermal capacitance is obtained by the initial warm-up slope after switching on the heater. After reaching equilibrium *i.e.* a few time constant, the thermal resistance is obtained by equation (11). Finally, The time constant, τ , is deduced from equation (3). Table 2 shows the measured thermodynamic properties and demonstrate that the predicted values from Table 1 are in good agreement with the measured data.

Table 2 : Measured thermal capacitance, C , thermal resistance, R and time constant τ .

C (J.K^{-1})	R (K.W^{-1})	τ (hours)
1330	7	2.6

Figure 4 shows a typical *in-situ* calibration cycle. The increase in the relative temperature, $\Delta(\text{TC}_i - \text{TC}_6)$ with $i = 1$ to 5, is plotted as a function of time when the heater is set to 0.1 W.m^{-1} and then to 0.02 W.m^{-1} . About 6 calibration measurements were performed, the average of the measured slopes is $2.7 \text{ K.W}^{-1}.\text{h}^{-1}$ which corresponds to a thermal capacitance of 1330 J.K^{-1} . In stable conditions, as demonstrated by the second increase in relative temperature, the apparatus sensitivity is, at least, 0.02 W.m^{-1} .

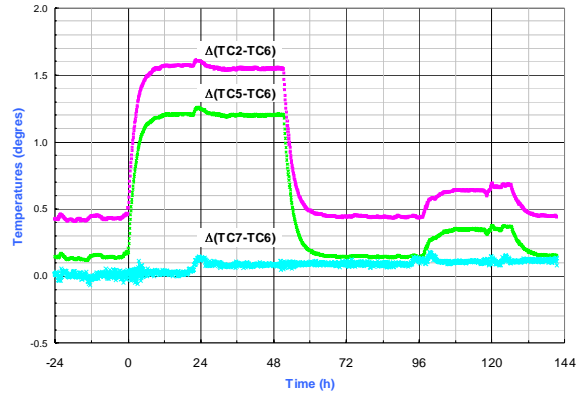


Figure 4 : Typical *in-situ* calibration cycle. The relative temperature increase correspond to 0.1 W/m and 0.02 W/m respectively. The average of the measured slopes is $2.7 \text{ K.W}^{-1}.\text{h}^{-1}$.

4 RESULTS

After commissioning of the experimental set-up several periods dedicated to electron cloud studies were performed with the SPS. We present here the very first observation of a temperature increase inside the calorimeter. Figure 5 shows the relative temperature and pressure increases, observed when LHC type beam was circulating in the calorimeter. The time-axis indicates the number of hours passed since recording. At time $< 115 \text{ h}$, the SPS was running with standard fixed target beams. During this period the pressure in the system was about $2 \cdot 10^{-9}$ Torr and only minor temperature variations were observed (TC2, TC3 and TC5), which were mainly due to temperature fluctuations in the SPS tunnel. The machine development (MD) period with LHC type beam started at time $= 115 \text{ h}$ and lasted until time $= 135 \text{ h}$. During this period, several pressure increases up to 10^{-7} Torr are observed. These pressure increases are due to electron stimulated desorption from electron multipacting. It should be noted that during this period the other SPS instrumentation devices such as pressure gauges, pick-ups, strip detectors, *etc.* also indicated electron cloud activity [10]. In general, the beam conditions were not stable all along this MD-period. However, a dedicated period with constant beam parameters over several hours (hour 133-135) could be obtained, enough time to determine the beam induced heat load. This beam was made of 3 consecutive batches separated by 225 ns of 72 bunches each, separated by 25 ns with $\sim 5 \cdot 10^{10}$ protons.bunch $^{-1}$ [10]. During this period a relative temperature increase, close to sensitivity limit, of about 0.2 degrees and significant pressure

increase is observed. From the measurement of the initial slope during the first hour of the electron cloud activity, a slope of ~ 0.075 degrees.h⁻¹ could be measured. This slope corresponds to a total deposited power onto the calorimeter of ~ 30 mW. At time > 135 h, the MD was completed and SPS was back to normal operation. The relative temperatures and pressure recover to their previous value before MD.

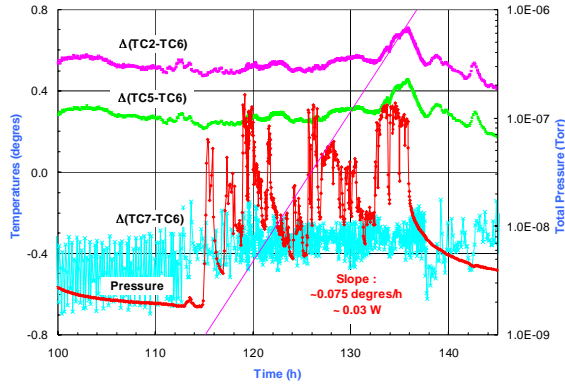


Figure 5 : Relative temperature and pressure observations when a LHC type beam of 3 consecutive batches of 72 bunches with $5 \cdot 10^{10}$ proton.bunch⁻¹ was circulating in the SPS.

Figure 6 shows the detail of the relative temperature increase observed during the electron cloud activity depicted in Figure 5. As mentioned in section 3.5, if the heat input is constant during a time larger than a few time constants, here about 1.5 time constants, the warm-up slope is almost equal to the final cool-down slope. The value of the two slopes are in relatively good agreement. The measure of the equilibrium temperature after 3 hours of operation gives a similar heat load as in the slope measurement case *i.e.* 40 to 60 mW/m .

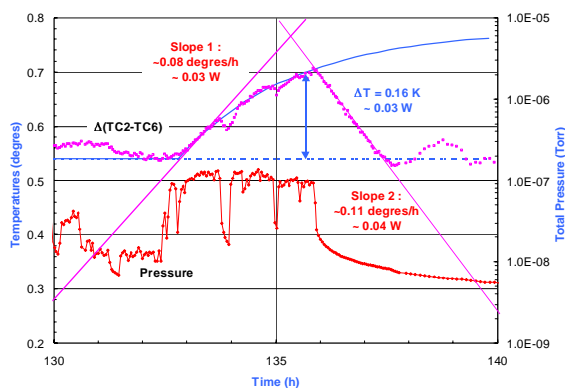


Figure 6 : Detail of the relative temperature increase observed during electron cloud activity of Figure 5.

5 BENCHMARKING SIMULATIONS

The measurements presented in 4 are used to benchmark two types of simulation code.

The “analytical” approach [1] computes the average kinetic energy of the electrons, moving along vertical field lines, kicked by a gaussian beam. This results in an average secondary electron yield $\langle \text{SEY} \rangle$ curve and an average electron energy as a function of radial position (Figure 7). Assuming that only the surface having a $\langle \text{SEY} \rangle$ above one *i.e.* from 0 to 5 mm in the present case, participates in the multipacting process and thus contribute to the heat load, their average energy is about 44 eV. If the electron cloud density is defined by its saturation limit, about 10^9 electron/m [11], the computed power is 68 mW/m in fairly good agreement with the measurements.

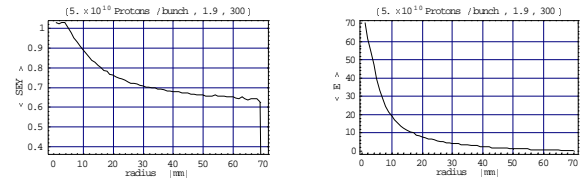


Figure 7 : Average secondary electron yield and average electron energy versus the radial position.

The “macroparticle” approach [12] follows the evolution of macroparticles through the 3 batches of proton bunches. All fundamental ingredients such as pressure, SEY curve, elastic reflection, space charge are included. Figure 8 shows the computed electron density in the Wampac during the passage of the LHC type beam. From the average energy of the electron cloud, the electron flux at saturation, the saturation time and the duty cycle, a power of 31 mW/m could be computed.

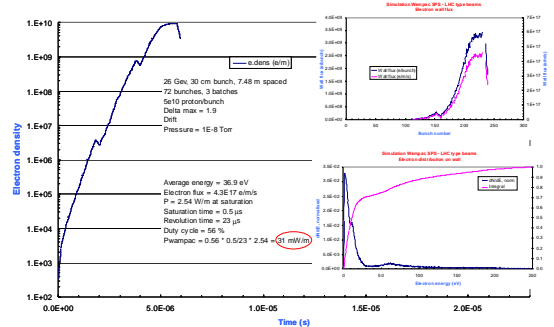


Figure 8 : Electron density, electron wall flux and electron energy in Wampac computed for a maximum secondary electron yield of 1.9.

Table 3 shows a compilation of several simulations performed with the beam parameters of paragraph 4 but without magnetic field for reasons of simplicity. It is shown that the measurements can be reasonably well obtained. A strong sensitivity is noted with the variation of the maximum of the SEY, δ_{max} .

Table 3 : Simulated power in Wampac as a function of the maximum of the SEY.

Pressure [Torr]	δ_{\max}	$\langle E \rangle$ [eV]	Flux [e/m/s]	Sat. Power [W/m]	Wampac Power [mW/m]
10^{-8}	1.90	36.9	$4 \cdot 10^{17}$	2.54	31
10^{-8}	1.95	32.9	$5 \cdot 10^{17}$	2.64	66
10^{-8}	2.00	29.2	$6 \cdot 10^{17}$	2.80	78

6 ESTIMATING LHC HEAT LOADS

The heat load measured with the calorimeter inside the SPS can be scaled to estimate the linear heat load into the LHC. If we assume that the electron cloud activity is nearly independent of the chamber diameter in the range 50 to 140 mm and of the dipole field in the range 0.5 to 8.5 T, only three corrections should be applied. 1) Since multipacting occurs only in the dipole a correction due to the dipole length, L , should be added, 2) the filling factor, f , and 3) the duty cycle, d , of the SPS should be taken into account. Under these assumptions, the LHC linear heat load, P_{LHC} , could be computed from the WAMPAC measurement, P_{Wampac} , by :

$$P_{\text{LHC}} = \frac{1}{L \times f \times d} P_{\text{Wampac}} \quad (13)$$

With the parameters from Figure 5, $L = 0.7$ m, $f = 2/11$ (three batch are circulating in the SPS but about one batch is required to trigger the electron cloud [9]), $d = 56$ % and $P_{\text{Wampac}} = 30$ to 40 mW, the estimated LHC heat load with $5 \cdot 10^{10}$ protons.bunch⁻¹ in a dipole region and a maximum secondary electron yield (SEY) of about 1.9 is [13] :

$$P_{\text{LHC}} \approx 0.4 \text{ to } 0.5 \text{ W.m}^{-1} \quad (14)$$

7 CONCLUSIONS

Preliminary measurements with the SPS calorimeter, WAMPAC, are presented. The calorimeter performance agrees with predictions. It has been demonstrated that a linear heat load of ~ 20 mW.m⁻¹ can be measured.

Under a dipole configuration, to reduce the electron cloud activity threshold, a power of 40 to 60 mW/m was measured when LHC type beams were circulating in the SPS. The measurements performed in the SPS are in good agreement with the code predictions.

The equivalent LHC linear heat load into the dipole was estimated to be ~ 0.5 W.m⁻¹ for a current of $5 \cdot 10^{10}$ protons.bunch⁻¹ and a Cu surface having a maximum secondary electron yield of ~ 1.9 .

To reduce the vertical aperture to 40 mm and simulate closer the LHC arc beam screen conditions, a new calorimeter has been installed during this shutdown in a SPS dipole chamber. Since predicted vertical electron stripes have been shown to exist [9],

this new calorimeter might be equipped, in the future, with a perforated copper screen and allow a direct measurement of the heat load which could be dissipated onto the LHC cold bore.

Finally, the COLDEX, an instrument to simulate as close as possible the arc beam vacuum system, was installed during this shutdown. Comparison of beam induced gas desorption, heat load deposited by a LHC type beam in a room temperature and in a cryogenic environment shall be performed.

8 ACKNOWLEDGEMENTS

The work performed, during the installation of WAMPAC in the SPS tunnel, by the LHC-VAC SL section and especially the team of G. Mathis is gratefully acknowledged. We would like to thank G. Arduini, the SL operation group and M. Jimenez for providing and coordinating the LHC type beams in the SPS. O. Gröbner, G. Rumolo and F. Zimmermann are acknowledged to allow the benchmarking of their code.

REFERENCES

- [1] Beam induced multipacting, O. Gröbner. LHC Project Report 127, July 1997.
- [2] Simulations for the beam induced electron cloud in the LHC beam screen with magnetic field and image charges, O. Brüning. LHC Project Report 158, November 1997.
- [3] The electron cloud effect in the arcs of the LHC, M. Furman. LHC Project Report 180, November 1998.
- [4] Electron cloud simulation an update, F. Zimmermann. Proceeding of XI Chamonix workshop, January 2001.
- [5] Advances in cryogenics at the Large Hadron Collider, P. Lebrun. LHC Project Report 211, July 1998.
- [6] Heat load working group home page, Main dipole nominal dynamic heat load last updated 26/3/01 by Th. Durand. <http://lhc-mgt-hlwg.web.cern.ch/lhc-mgt-hlwg/>
- [7] Electron cloud : SPS observations with LHC type beams, G. Arduini, K. Cornelis, J. M. Jimenez, G. Moulard, M. Pivi and K. Weiss. Proceeding of X Chamonix workshop, January 2000.
- [8] Estimation of thermal resistance from room temperature electrical resistance measurements for different LHC beam screen support systems, B. Jenninger. LHC Project Note 189, May 1999.
- [9] M. Jimenez, LHC Machine Advising Committee 12/11/01.
- [10] M. Jimenez, private communication 27/11/01.
- [11] Electron cloud : an analytic view, L. Vos. LHC project note 150, 1998.

- [12] G. Rumolo and F. Zimmermann, these proceedings.
- [13] B. Henrist, private communication 27/11/01. The secondary electron yield measurement device is installed in SPS sector 520 where most of the time a dipole field of 70 gauss is applied. The measurement was performed just before (24/10/01, 0h22) and after (25/10/0, 8h511) the MD period and the SEY did not change appreciably during this period.